PCCP

RSC Publishing

PAPER

High hydrostatic pressure effects investigated by neutron scattering on lipid multilamellar vesicles

Cite this: *Phys. Chem. Chem. Phys.*, 2013, **15**, 20951

Marcus Trapp,[ab] Jérémie Marion,[cde] Moeava Tehei,[fg] Bruno Demé,[d] Thomas Gutberlet[b] and Judith Peters*[cde]

Received 2nd July 2013,
Accepted 25th October 2013

DOI: 10.1039/c3cp52762j

www.rsc.org/pccp

The effects of high hydrostatic pressure on the structure and dynamics of model membrane systems were investigated using neutron scattering. Diffraction experiments show shifts of the pre- and main-phase transitions of multilamellar vesicles of 1,2-dimyristoyl-*sn-glycero*-3-phosphocholine (DMPC) to higher temperatures with increased pressure which are close to results observed previously by other techniques, namely (10.4 ± 1.0) K kbar^{-1} and (20.0 ± 0.5) K kbar^{-1} for the two transitions. Backscattering spectroscopy reveals that the mean square displacements in the liquid phase are about 10% smaller at 300 bar and about 20% smaller at 600 bar compared to atmospheric pressure, whereas in the gel phase below the main phase transition the mean square displacements show a smaller difference in the dynamics of the three pressure values within the studied pressure range.

1. Introduction

Life as we know it takes place on the surface of the earth, but about 75% of the biosphere lies at a depth of 1000 m sea level or even below. This corresponds to a pressure of 100 bar or more (1 bar = 0.1 MPa), hence life has to find strategies to adapt to these extreme conditions. It was found that membranes are particularly sensitive to pressure changes.[1] Lipids are essential components of cell membranes and undergo several transitions between different lamellar states. The commonly observed L_c lamellar crystalline phase is the most ordered one at low temperature, but will not be investigated in the experiments presented here. In the $L_{\beta'}$ phase, the 'gel' phase, the lipid chains are ordered in the all-*trans* configuration. The prime indicates that the alkyl chains are tilted with respect to the bilayer normal. The high degree of chain order leads to a quasi-crystalline order. The $P_{\beta'}$ phase or 'ripple' phase is formed prior to the main phase transition. It exhibits one dimensional ripples on the membrane surface. Close to the main phase transition, a co-existence as rafts of L_α domains in a $P_{\beta'}$ continuum and of $P_{\beta'}$ domains in a L_α continuum with increasing temperature was observed.[2] Finally the L_α phase, the liquid-disordered or fluid phase, corresponds to the physiological state in cells. Indeed, the higher flexibility in this phase permits the membranes to accomplish their biological function.

High hydrostatic pressure (HHP) increases not only the order of the lipid chains and therefore the temperatures of the phase transitions, but also the number of possible phases can be increased under specific conditions. One way to counteract the rigidifying effect of HHP to maintain membranes in the physiological state is the incorporation of lipids with unsaturated chains or of molecules that increase the membrane fluidity. In fact, the cells have the capacity to adapt the lipid composition of their membranes by a metabolic response. The kinked chain of unsaturated lipids decreases the chain ordering and thus lowers the transition temperature T_m[3] helping in this way the organisms to survive under HHP conditions. Higher concentrations of unsaturated lipids were indeed found in organisms from the deep sea.[4,5]

Membrane fluidity plays also a key role in the activity of membrane bound proteins. For instance, the activity of the multi-drug resistant transporters LmrA[6] and HorA[7] strongly depends on the phase behavior of the surrounding lipids. The gel phase, induced by HHP, leads to a drastic inhibition of the transporters and consequent cell death. HHP was also used in food processing and preservation. For instance, pressure of up to 6 kbar is used to inactivate microorganisms and enzymes while sensorial characteristics are preserved.[8]

Structural investigations using neutron diffraction in combination with high hydrostatic pressure have been performed quite a while ago for single component membranes,[5,9,10] also a

[a] *Angewandte Physikalische Chemie, Universität Heidelberg, Im Neuenheimer Feld 253, 69120 Heidelberg, Germany*
[b] *Helmholtz-Zentrum Berlin für Materialien und Energie, Lise-Meitner Campus, Hahn-Meitner-Platz 1, 14109 Berlin, Germany*
[c] *Institut de Biologie Structurale, 41 rue Jules Horowitz, 38027 Grenoble Cedex 1, France. E-mail: peters@ill.fr*
[d] *Institut Laue-Langevin, 6 rue Jules Horowitz, BP 156, 38042 Grenoble Cedex 9, France*
[e] *University Joseph Fourier, UFR PhITEM, BP 53, 38041 Grenoble Cedex 9, France*
[f] *University of Wollongong, School of Chemistry, NSW 2522, Australia*
[g] *Centre for Medical Bioscience, Australian Institute of Nuclear Science and Engineering (AINSE), Menai, NSW, Australia*

variety of small angle studies of single and multicomponent membranes can be found in the literature.[11,12]

In contrast to structural investigations, incoherent neutron scattering studies focus on the dynamics of the system under investigation. Compared to structural information available, the knowledge of the dynamical behavior of biomolecules under HHP and especially membranes is still scarce.[13–15] This fact can be attributed to experimental challenges combining high pressure with spectroscopic neutron techniques, but also to the increased measuring times when comparing coherent with incoherent techniques.

To shed light on the potential of incoherent neutron scattering for such explorations, we have studied single component model membranes of 1,2-dimyristoyl-*sn-glycero*-3-phosphocholine (DMPC), a system which allows us to compare our findings with results obtained by other techniques such as differential scanning calorimetry (DSC) or molecular dynamics (MD) simulations.[16,17] Here we investigated first the phase behavior of DMPC as a function of pressure and temperature using neutron diffraction and small angle neutron scattering (SANS) measurements. Second, elastic incoherent neutron scattering was employed in order to study the dynamical response to pressure.

The neutron diffraction measurements confirmed results close to earlier measurements mentioned above.

In addition, we correlated the structural changes with atomic mean square displacements (MSDs) extracted from neutron backscattering experiments to study the influence of HHP on the molecular dynamics level. The MSDs revealed a reduction under HHP compared to ambient conditions and a sudden rise linked to the phase transitions.

2. Materials and methods

2.1 Sample preparation

Fully protonated DMPC powder was purchased from Lipoid GmbH (Ludwigshafen, Germany) and used as received. For the neutron experiments, lipid powder was hydrated in a desiccator from a pure D_2O atmosphere for at least two days at 40 °C.[18] In order to assure fully hydrated multilamellar vesicles (MLVs) and a homogeneous pressure transmission, D_2O was added after filling the pressure cell with the hydrated lipids. DSC measurements were performed before and after the neutron experiments (results not shown), in both cases the data showed the well-known phase diagram of DMPC.

2.2 High pressure cell

A cylindrical pressure cell made of a high-tensile aluminum alloy (7049-T6), a material which is mainly transparent for neutrons, was especially developed for neutron experiments. The cell consists of a cylinder with an inner diameter of 6 mm and an outer diameter of 10 mm, leading to a thickness of 4 mm and a maximum pressure capacity of 1.5 kbar. The sample volume was reduced using a cylindrical aluminum insert of 4 mm diameter. A detailed description of the pressure cells and the high pressure equipment can be found in Peters *et al.*[19] Technical test experiments were successful, and the present investigations with model membranes were part of this process.

2.3 Neutron scattering measurements

Diffraction measurements of DMPC were performed at the instrument D16 of the ILL.[20] The incident wavelength was set to 4.75 Å and small momentum transfers Q (between 0.05 and 0.15 $Å^{-1}$) were recorded to access typical repeat distances d (about 60 Å and more). The temperature was controlled using a cryofurnace. Temperature scans in the range from 280 to 320 K were recorded in steps of 1 K at three different pressure values, ambient pressure, 300 and 600 bar. The temperature domain covered thus the gel, the ripple and the fluid phases of the lipids. The sample was equilibrated for 10 minutes at each temperature prior to the 15 minutes data recording. With a second pressure cell it was possible to reach values up to 6 kbar. The corresponding diffraction data will be presented in a later publication.

The thermal backscattering spectrometer IN13 at ILL[21,22] was used to explore the dynamics of DMPC. Its instrumental elastic energy resolution of $\Delta E \approx 8$ μeV gives access to a pico- to nanosecond timescale for the molecular dynamics whereas the space window comprises a few Ångstrom. The time window allows us only to probe small local motions, but it has been shown experimentally[23] and by simulations[24,25] that for biological systems a hierarchy of motions exists. Thus movements at different time scales correlate and span over many orders of magnitude from bond vibrations on the femto-second scale up to large domain motions on the millisecond scale. Fixed energy window (FEW) scans were recorded in a temperature range from 285 to 318 K at the same three pressure values used on D16. After 15 minutes of equilibration, typical counting times were 6 h in the gel phase and 10 h in the liquid phase. For data correction also the empty high pressure cell, the cell filled with D_2O as well as the cell filled with a vanadium sheet were measured.

Data reduction was performed using the Large Array Manipulation Program (LAMP) available at the ILL.[26] Absorption, self-shielding and multiple scattering corrections were calculated for the dynamics measurements using a program developed by Petrillo *et al.*[27,28] The program described in the articles was originally written for the analysis of neutron diffraction data collected for a sample in a complex cell made of n concentric cylinders and later on modified for data collected in the same type of cell for the analysis of elastic and quasi-elastic scattering data. The latter version was used for our analysis.

Elastic incoherent neutron scattering data are analyzed through the scattering function $S(Q,0 \pm \Delta E)$. Assuming a normal distribution of the atoms around their average position it reduces in terms of the Gaussian approximation[29–31] to:

$$S(Q, 0 \pm \Delta E) \approx \exp\left(-\frac{1}{3}Q^2\langle u^2\rangle\right). \quad (1)$$

Here $\langle u^2\rangle$ are the average atomic mean-square displacements (MSD). The MSD values are obtained for each temperature/pressure point from the slope of the logarithm of the scattered intensities $S(Q, 0 \pm \Delta E)$ plotted *versus* Q^2 according to

$$\langle u^2\rangle = -3\frac{\partial \ln S(Q, 0 \pm \Delta E)}{\partial Q^2}. \quad (2)$$

This approximation is strictly speaking only valid for $Q \rightarrow 0$, but can be extended to $\langle u^2 \rangle\, Q^2 < 1$.[32] Accordingly, in this study the fit range was restricted to the linear range in the low Q regime between 0.55 $Å^{-1}$ and 1.47 $Å^{-1}$.

Incoherent neutron scattering is largely dominated by hydrogen atoms, because their incoherent scattering cross section is much higher than the signal of any other type of atom present in biological samples.[33] The MSDs thus reflect the averaged atomic motion of hydrogen atoms, which are mostly homogeneously distributed in biological macromolecules and inform in a first approach over local atomic vibrations. They are associated with the sample flexibility[34] *via* the fluctuation–dissipation theorem.[35]

An effective mean force constant, representing the resilience of the system against temperature changes, can be calculated from the MSDs through

$$\langle k_{\mathrm{eff}} \rangle = 0.00138 \left(\frac{\mathrm{d}\langle u^2 \rangle}{\mathrm{d}T} \right)^{-1} \qquad (3)$$

according to ref. 36. $\langle k_{\mathrm{eff}} \rangle$ is obtained in units of N m^{-1}, when the $\langle u^2 \rangle$ are in $Å^2$ and T is in Kelvin.

The accessible window in time and space depends on the instrumental resolution and the available Q-range, respectively. In the case of IN13 the observation time lies around 100 ps for a length scale between about 1 and 30 Å. Thus local motions are the aim of our investigation. Obviously, such motions within the lipid chains are particularly sensitive to pressure, as phase transitions correspond mainly to a rearrangement of the chains and are translated through a sudden increase of the MSDs.

3. Results

3.1 Neutron diffraction

After calibration the data were radially integrated. The repeat distance d was calculated according to Bragg's law

$$d = \frac{2\pi}{Q} \qquad (4)$$

fitting a Gaussian curve to the first order Bragg peaks. At the pre-transition a sudden increase in d from 60 to about 70 Å was observed (Fig. 1). Corresponding values for the temperature of the pre-transition T_{p} can be found in Table 1.

The increased value of d in the $P_{\beta'}$ phase is caused by the formation of ripples in the plane of the bilayer.[38] The jump in d is slightly less pronounced with increasing pressure. Winter and Jeworrek[11] state that the compression of a bilayer would provoke a lateral shrinking and an increase in thickness. However, this is not reflected in the d-spacings measured on D16. A possible explanation can be a reduced inter-bilayer water thickness due to the elevated hydrostatic pressure.[39] This finding is also supported by hydration dependent results from quasi-elastic and elastic incoherent neutron scattering on DMPC,[40,41] where T_{m} is shifted as well to higher temperatures as the dynamics are hindered due to insufficient hydration. At temperatures higher than the pre-transition, the repeat distances decrease during melting at the $P_{\beta'}/L_{\alpha}$-transition,

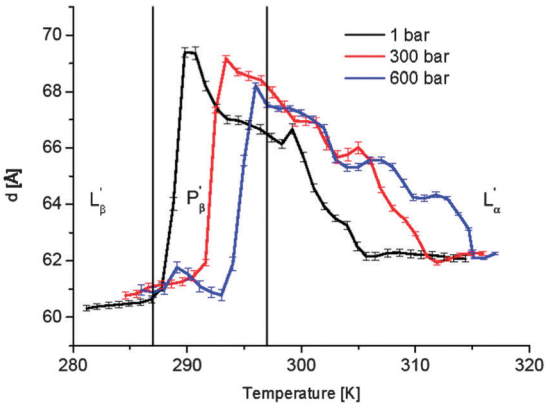

Fig. 1 Repeat distance d for DMPC MLVs as a function of temperature and pressure. Lines are guide to the eyes. The two vertical black lines indicate the literature values for the two phase transition temperatures at atmospheric pressure. As the neutron experiments were carried out in D_2O the transition temperatures are shifted to higher values compared to H_2O.[37]

Table 1 Temperatures of the pre- (T_{p}) and main (T_{m}) phase transition for pure DMPC. Also given the repeat distance closely above the pre-transition and well above the main phase transition. Note that d after the pre-transition decreases with pressure, whereas d in the L_{α} phase stays constant

Pressure (bar)	T_{p} (K)	d after pre-transition (Å)	T_{m} (K)	d in the L_{α} phase (Å)
1	290	69.4 ± 0.2	297	62.2 ± 0.1 (314 K)
300	293	69.2 ± 0.1	303	62.3 ± 0.1 (316 K)
600	296	68.2 ± 0.1	309	62.1 ± 0.1 (316 K)

and drops at the main phase transition, until a constant value for d is reached in the liquid phase. The values for d in the L_{α} phase at 315 K for the three different pressure values show a value around 62.2 Å. A typical value for the repeat distance of fully hydrated DMPC in the liquid phase at ambient pressure found *e.g.* with X-ray scattering lies around 62.6 Å.[42]

Fig. 2 shows values for T_{p} and T_{m} as a function of pressure. From linear fits to the data, values of $\mathrm{d}T_{\mathrm{p}}/\mathrm{d}p$ of (10.4 ± 1.0) K/1000 bar and $\mathrm{d}T_{\mathrm{m}}/\mathrm{d}p$ of (20.0 ± 0.5) K/1000 bar were obtained, which are close to values given in the literature and extracted through various experimental techniques.[10,12,43–46]

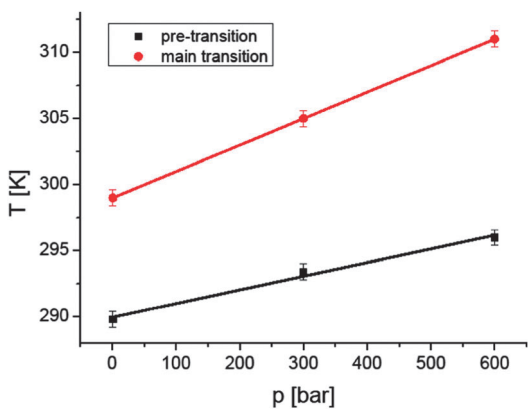

Fig. 2 p, T phase diagram of DMPC MLVs in excess of D_20.

3.2 Spectroscopy

3.2.1 Elastic neutron scattering. Fig. 3 represents the raw data of the elastic neutron intensities for DMPC summed over all accessible scattering angles (corresponding to a range of 0.29 $Å^{-1} < Q <$ 4.98 $Å^{-1}$). Data were corrected for multiple scattering and normalized to vanadium. In contrast to the MSDs, where the Gaussian approximation has to be fulfilled, the integrated intensities are not restricted to the Q-region below 1.47 $Å^{-1}$. The slopes of the summed intensities show no change around the transition from the gel to ripple phase, whereas a drastic decrease in intensity can be observed around the main phase transition. The drop in intensity at the main phase transition becomes less pronounced with increasing pressure, hence the molecular flexibility is reduced. This is also underlined by the increase of the elastic intensity with increasing pressure, showing that the atoms are more confined, moving less and thus scattering the neutrons more elastically.

3.2.2 Mean square displacements. Contrary to the summed elastic intensities the MSDs decrease with pressure. The results for DMPC MLVs including all corrections (absorption, self-shielding and multiple scattering) are shown in Fig. 4. Multiple scattering corrections showed a negligible effect compared to self-shielding and absorption. The same was found for elastic scans of membrane systems reported by Busch *et al.*[47]

Again no change in the slope of the MSDs is observed around the pre-transition. The main phase transition, where the $\langle u^2 \rangle$ show a sudden jump to higher values, is shifted to higher temperatures as pressure is raised. The jump in the dynamics is clearly correlated with the main phase temperature and both show the same evolution to higher temperatures under pressure. As the MSDs are associated with the sample flexibility, the transition stands for a measure of the fluctuations in this temperature region, as explained in more detail in a publication by M. Rheinstädter *et al.*[48] The absolute values of the MSDs are reduced in the liquid phase with increasing pressure indicating more confined motions under pressure.

Using time resolved fluorescence spectroscopy Bernsdorff *et al.* found an increase in fluorescence lifetime at the pressure induced phase transition of DPPC. This effect was interpreted as a greater headgroup hydration in the liquid-crystalline phase due to an increased disorder. Hence, pressure induces a dehydration of the headgroup which results in a reduced mobility of the lipids.[39]

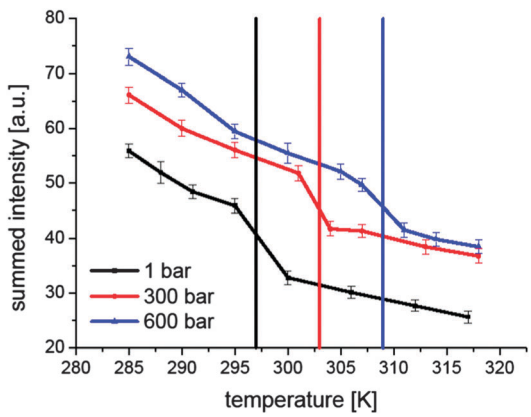

Fig. 3 Summed elastic intensities of DMPC on IN13. Data are summed over the complete Q-range available on IN13 (0.29 $Å^{-1} < Q <$ 4.98 $Å^{-1}$). Vertical lines indicate the temperature of the corresponding main phase transition in the color corresponding to the data points. Lines connecting the data points are guide to the eyes.

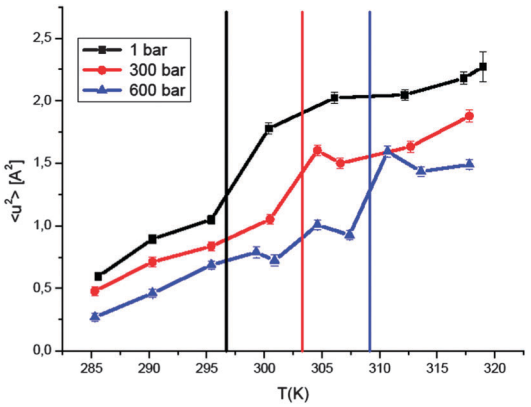

Fig. 4 Mean square displacements of DMPC calculated according to eqn (2). Vertical lines indicate the temperature of the main phase transition at the corresponding pressure and the corresponding color, respectively; lines connecting the data points are guide to the eyes.

Table 2 Effective force constants calculated for DMPC below and above the main phase transition temperature. The value of k_{eff} above T_m at 600 bar was obtained from a fit of only two points. Therefore, no error is given

Pressure (bar)	$\langle k_{eff} \rangle$ below T_m (N m^{-1})	$\langle k_{eff} \rangle$ above T_m (N m^{-1})
1	0.015 ± 0.002	0.025 ± 0.010
300	0.019 ± 0.003	0.021 ± 0.003
600	0.017 ± 0.002	0.051

Effective mean force constants were extracted according to eqn (3), which account for the resilience of the sample below and above the main phase transition (see Table 2). The values are extremely low compared to typical numbers for biological membranes, proteins or lipoproteins,[49–51] thus corresponding to a very high flexibility of the sample.

The force constants extracted from our elastic measurements are almost equal within error bars in the gel and the fluid phase ranging between 0.015 and 0.025 N m^{-1} indicating that the increase of the MSDs is linear and nearly equal in both regimes due to the rise of thermal energy in the system. Only around the main phase transition the dynamics is thus enhanced due to higher fluctuations. A very slight tendency to higher force constants at all pressure values in the fluid phase compared to the gel phase is noticed. We speculate that this reduction in the dynamics in the liquid phase even if it stays within the error bars of the experiment is due to a higher degree of order induced by the applied high pressure. The sample stability shows almost no pressure dependence in the pressure range investigated here.

4. Results

4.1 Neutron diffraction

The main phase transition as a function of pressure has been investigated over years by a number of independent techniques

such as *e.g.* electron paramagnetic resonance,[43] dilatometry,[44,45] light transmittance[10,46] and SANS/SAXS.[11,12] All of these studies find values for dT_m/dp in the range of 20 K kbar^{-1} to 25 K kbar^{-1}, typical for melting phenomena of hydrocarbon chains[52] and only slightly depending on their exact chain length.[44] Krishna Prasad and coworkers[10] and Ichimori *et al.*[46] found slopes for the pre-transition of DMPC dT_p/dp ranging from 12 to 14 K kbar^{-1}. Thus our values obtained from linear fitting the data in Fig. 2 agree with the values found in the literature. The slightly smaller values extracted here may be due to the small number of data points in this study compared to other methods and to inertia of the lipids against temperature changes. The results obtained by neutron diffraction thus reproduce the values checked independently between many experimental techniques and characterize the sample for the neutron spectroscopy measurements.

4.2 Neutron spectroscopy

Summed elastic intensities of DMPC measured on IN13 are shown in Fig. 3. The pre-transition from the gel to ripple phase is neither visible in the integrated elastic intensities nor in the mean square displacements (*cf.* Fig. 3 and 4). This reflects the fact that the pre-transition does not have a detectable influence on the system fluctuations in the observed time and space window. In contrast, the main phase transition is clearly visible as a sudden drop of intensity (see Fig. 3) and a sudden increase of the MSDs (see Fig. 4) indicating an enhanced flexibility of the system in the liquid phase, which is, however, coupled to a higher stability as established by the increased force constant in that state.

The higher intensity with rising pressure observed in Fig. 3 may have two reasons: (1) the increased amount of scattering centers in the beam, due to the compression of the sample or (2) the motion of hydrogen atoms, which contribute with about 94% to the incoherent scattering from the lipids, enters the time window of the spectrometer under HHP. The first point was investigated by transmission measurements performed at 285 K for all three pressure values. Within experimental errors the obtained transmission values agreed for all pressures, thus the number of scattering centers in the neutron beam stays constant. The second point and according to Le Chatelier's principle, an increase in pressure provokes a decrease in volume and thus a damping of atomic motions.[53] Therefore, hydrogen atoms which do not contribute at atmospheric pressure to the elastic, but to the quasi-elastic signal enter the elastic space-time window of IN13 at elevated pressure, hence the elastic intensity increases. Moreover, this fact can be an explanation for the less pronounced drop of elastic intensity at the main phase transition with increasing pressure seen in Fig. 3. The applied pressure reduces the mobility of the hydrogen and therefore increases the elastic signal.

Similar trends can be observed for the mean square displacements shown in Fig. 4. Due to the densely packed lipid chains below the main phase transition the pressure effect on the dynamics in the gel and ripple phase is indeed minimal compared to the effect in the liquid phase, which can be seen from the fact that the MSDs just below the transition show similar values in contrast to values above T_m.

5. Conclusions

The current study investigated the influence of hydrostatic pressure on the structure and dynamics of the model membrane system DMPC. Neutron diffraction was used to address structural aspects, whereas neutron backscattering spectroscopy was employed to probe the dynamics in the pico- to nanosecond time range. Both methods proved the potential of neutron scattering approaches to study temperature and HHP effects on biomolecules. In agreement with previous studies the diffraction data showed a shift of the main phase transition of (20.0 $\pm$ 0.5) K/1000 bar and of the pre-transition of (10.4 $\pm$ 1.0) K/1000 bar. The external hydrostatic pressure shows a similar effect as reduced hydration on membranes,[40,41] both limiting the possible motions of the lipids.

Neutron spectroscopy showed that the atomic mean square displacements under HHP are about 10–20% smaller than at atmospheric pressure. The results serve as a benchmark for future experiments and simulations addressing in particular pressure effects on natural membranes and membrane–protein complexes and may clarify the role the membrane matrix plays *e.g.* in combination with protein deactivation upon applying pressure. Looking at other techniques, such as NMR,[54–59] where high pressure techniques became accessible earlier, a wide field of applications in protein[60] and membrane biophysics can be addressed in the future.

Acknowledgements

We acknowledge the ILL for the allocation of beam time in the framework of a long term proposal. M. Trapp was supported by a PhD scholarship from the French Ministry for Research and Technology. M. Tehei acknowledges the financial support from the Access to Major Research Facilities Program which is a component of the International Science Linkages Program established under the Australian Government's innovation statement, Backing Australia's Ability. We thank P. Masson for his careful reading of the manuscript and his precious advices. We are grateful to the SANE group of the ILL and particularly to J.-L. Laborier and C. Payre for building the pressure cell and for their technical support with the high pressure equipment.

Notes and references

1 G. N. Somero, *Annu. Rev. Physiol.*, 1992, **54**, 557–577.
2 C. L. Armstrong, M. A. Barrett, L. Toppozini, N. Kucerka, Z. Yamani, J. Katsaras, G. Fragneto and M. C. Rheinstädter, *Soft Matter*, 2012, **8**, 4687–4694.
3 D. H. Bartlett, *Biochim. Biophys. Acta, Protein Struct. Mol. Enzymol.*, 2002, **1595**, 367–381.
4 A. R. Cossins and A. G. Macdonald, *Biochim. Biophys. Acta Biomembr.*, 1986, **860**, 325–335.
5 P. T. T. Wong, D. J. Siminovitch and H. H. Mantsch, *Biochim. Biophys. Acta, Rev. Biomembr.*, 1988, **947**, 139–171.

6 H. Teichert, N. Periasamy, R. Winter and R. F. Vogel, *High Pressure Res.*, 2009, **29**, 344–357.
7 H. M. Ulmer, H. Herberhold, S. Fahsel, M. G. Ganzle, R. Winter and R. F. Vogel, *Appl. Environ. Microbiol.*, 2002, **68**, 1088–1095.
8 M. L. M. Lopes, V. L. Valente Mesquita, A. C. N. Chiaradia, A. A. R. Fernandes and P. M. B. Fernandes, *Ann. N. Y. Acad. Sci.*, 2010, **1189**, 6–15.
9 L. F. Braganza and D. L. Worcester, *Biochemistry*, 1986, **25**, 2591–2596.
10 S. Krishna Prasad, R. Shashidhar, B. P. Gaber and S. C. Chandrasekhar, *Chem. Phys. Lipids*, 1987, **43**, 227–235.
11 R. Winter and C. Jeworrek, *Soft Matter*, 2009, **5**, 3157–3173.
12 R. Winter and W.-C. Pilgrim, *Ber. Bunsen-Ges.*, 1989, **93**, 708–717.
13 A. Filabozzi, A. Deriu, M. T. Di Bari, D. Russo, S. Croci and A. Di Venere, *Biochim. Biophys. Acta, Proteins Proteomics*, 2010, **1804**, 63–67.
14 M. G. Ortore, F. Spinozzi, P. Mariani, A. Paciaroni, L. R. S. Barbosa, H. Amenitsch, M. Steinhart, J. Ollivier and D. Russo, *J. R. Soc., Interface*, 2009, **6**, S619–S634.
15 W. Doster and R. Gebhardt, *Chem. Phys.*, 2003, **292**, 383–387.
16 M. J. Janiak, D. M. Small and G. G. Shipley, *J. Biol. Chem.*, 1979, **254**, 6068–6078.
17 B. Griepernau and R. A. Böckmann, *Biophys. J.*, 2008, **95**, 5766–5778.
18 S. Busch, C. Smuda, L. C. Pardo and T. Unruh, *J. Am. Chem. Soc.*, 2010, **132**, 3232–3233.
19 J. Peters, M. Trapp, D. Hughes, S. Rowe, B. Demé, J.-L. Laborier, C. Payre, J.-P. Gonzales, S. Baudoin, N. Belkhier and E. Lelievre-Berna, *High Pressure Res.*, 2011, **32**, 97–102.
20 http://www.ill.eu/instruments-support/instruments-groups/instruments/d16/.
21 http://www.ill.eu/instruments-support/instruments-groups/instruments/in13/description/instrument-layout/.
22 F. Natali, J. Peters, D. Russo, S. Barbieri, C. Chiapponi, A. Cupane, A. Deriu, M. T. Di Bari, E. Farhi, Y. Gerelli, P. Mariani, A. Paciaroni, C. Rivasseau, G. Schirò and F. Sonvico, *Neutron News*, 2008, **19**, 14–18.
23 K. Henzler-Wildman and D. Kern, *Nature*, 2007, **450**, 964–972.
24 G. R. Kneller and K. Hinsen, *J. Chem. Phys.*, 2004, **121**, 10278–10283.
25 G. R. Kneller, *Phys. Chem. Chem. Phys.*, 2005, **7**, 2641–2655.
26 http://www.ill.eu/data_treat/lamp/the-lamp-book/.
27 C. Petrillo and F. Sacchetti, *Acta Crystallogr., Sect. A: Fundam. Crystallogr.*, 1990, **46**, 440–449.
28 C. Petrillo and F. Sacchetti, *Acta Crystallogr., Sect. A: Fundam. Crystallogr.*, 1992, **48**, 508–515.
29 A. Guinier and G. Fournier, *Small-angle scattering of X-rays*, John Wiley & Sons, Inc., Hoboken, New Jersey, USA, 1955.
30 A. Rahman, K. S. Singwi and A. Sjölander, *Phys. Rev.*, 1962, **126**, 986–996.
31 F. Gabel, D. Bicout, U. Lehnert, M. Tehei, M. Weik and G. Zaccai, *Q. Rev. Biophys.*, 2003, **35**, 327–367.
32 V. Réat, G. Zaccai, C. Ferrand and C. Pfister, *Functional Dynamics in Purple Membranes*, 1997.
33 V. F. Sears, *Neutron News*, 1992, **3**, 26–37.
34 G. Zaccai, *J. Non-Cryst. Solids*, 2011, **357**, 615–621.
35 H. B. Callen and T. A. Welton, *Phys. Rev.*, 1951, **83**, 34–40.
36 G. Zaccai, *Science*, 2000, **288**, 1604–1607.
37 G. Lipka, B. Z. Chowdhry and J. M. Sturtevant, *J. Phys. Chem.*, 1984, **88**, 5401–5406.
38 J. Eisenblätter and R. Winter, *Biophys. J.*, 2006, **90**, 956–966.
39 C. Bernsdorff, A. Wolf, R. Winter and E. Gratton, *Biophys. J.*, 1997, **72**, 1264–1277.
40 M. Trapp, F. Juranyi, M. Tehei, L. van Eijck, B. Demé, T. Gutberlet and J. Peters, *Spectroscopy*, 2010, **24**, 461–466.
41 M. Trapp, T. Gutberlet, F. Juranyi, T. Unruh, B. Demé, M. Tehei and J. Peters, *J. Chem. Phys.*, 2010, **133**, 164505–164507.
42 N. Kucerka, Y. Liu, N. Chu, H. I. Petrache, S. Tristram-Nagle and J. F. Nagle, *Biophys. J.*, 2005, **88**, 2626–2637.
43 J. R. Trudell, D. G. Payan, J. H. Chin and E. N. Cohen, *Proc. Natl. Acad. Sci. U. S. A.*, 1975, **72**, 210–213.
44 J. F. Nagle and D. A. Wilkinson, *Biophys. J.*, 1978, **23**, 159–175.
45 A. G. Macdonald, *Biochim. Biophys. Acta Biomembr.*, 1978, **507**, 26–37.
46 H. Ichimori, T. Hata, H. Matsuki and S. Kaneshina, *Biochim. Biophys. Acta Biomembr.*, 1998, **1414**, 165–174.
47 S. Busch and T. Unruh, *J. Phys.: Condens. Matter*, 2011, **23**, 254205.
48 M. C. Rheinstädter, T. Seydel, F. Demmel and T. Salditt, *Phys. Rev. E: Stat., Nonlinear, Soft Matter Phys.*, 2005, **71**, 061908.
49 G. Nagy, J. Pieper, S. Krumova, L. Kovacs, M. Trapp, G. Garab and J. Peters, *Photosynth. Res.*, 2012, **111**, 113–124.
50 K. Wood, U. Lehnert, B. Kessler, G. Zaccai and D. Oesterhelt, *Biophys. J.*, 2008, **95**, 194–202.
51 C. Mikl, J. Peters, M. Trapp, K. Kornmueller, W. J. Schneider and R. Prassl, *J. Am. Chem. Soc.*, 2011, **133**, 13213–13215.
52 A. Würflinger and G. M. Schneider, *Ber. Bunsen-Ges.*, 1973, **77**, 121–128.
53 L. Meinhold, J. C. Smith, A. Kitao and A. H. Zewail, *Proc. Natl. Acad. Sci. U. S. A.*, 2007, **104**, 17261–17265.
54 X. Peng and J. Jonas, *Biochemistry*, 1992, **31**, 6383–6390.
55 X. Peng, A. Jonas and J. Jonas, *Biophys. J.*, 1995, **68**, 1137–1144.
56 B.-S. Lee, S. A. Mabry, A. Jonas and J. Jonas, *Chem. Phys. Lipids*, 1995, **78**, 103–117.
57 J. Jonas, C. L. Xie, A. Jonas, P. J. Grandinetti, D. Campbell and D. Driscoll, *Proc. Natl. Acad. Sci. U. S. A.*, 1988, **85**, 4115–4117.
58 J. Jonas and A. Jonas, *Annu. Rev. Biophys. Biomol. Struct.*, 1994, **23**, 287–318.
59 J. Eisenblätter, A. Zenerino and R. Winter, *Magn. Reson. Chem.*, 2000, **38**, 662–667.
60 J. Roche, J. Ying, A. S. Maltsev and A. Bax, *ChemBioChem*, 2013, **14**, 1754–1761.

